Deformation of Platonic foam cells: Effect on growth rate

Myfanwy E. Evans,[1] Johannes Zirkelbach,[1] Gerd E. Schröder-Turk,[1,*] Andrew M. Kraynik,[1,2] and Klaus Mecke[1,†]
[1]*Theoretische Physik, Friedrich-Alexander Universität Erlangen-Nürnberg, Staudtstr. 7B, 91058 Erlangen, Germany*
[2]*Chemical Engineering and Analytical Science, University of Manchester, Oxford Rd, Manchester, M13 9PL, UK*
(Received 2 February 2012; published 1 June 2012)

The diffusive growth rate of a polyhedral cell in dry three-dimensional foams depends on details of shape beyond cell topology, in contrast to the situation in two dimensions, where, by von Neumann's law, the growth rate depends only on the number of cell edges. We analyze the dependence of the instantaneous growth rate on the shape of single foam cells surrounded by uniform pressure; this is accomplished by supporting the cell with films connected to a wire frame and inducing cell distortions by deforming the wire frame. We consider three foam cells with a very simple topology; these are the *Platonic* foam cells, which satisfy Plateau's laws and are based on the trivalent Platonic solids (tetrahedron, cube, and dodecahedron). The Surface Evolver is used to model cell deformations induced through extension, compression, shear, and torsion of the wire frames. The growth rate depends on the deformation mode and frame size and can increase or decrease with increasing cell distortion. The cells have negative growth rates, in general, but dodecahedral cells subjected to torsion in small wire frames can have positive growth rates. The deformation of cubic cells is demonstrated experimentally.

DOI: 10.1103/PhysRevE.85.061401 PACS number(s): 82.70.Rr

I. INTRODUCTION

Foams are complex fluids consisting of gas bubbles dispersed in a small amount of liquid and separated by thin films that are stabilized by surfactants. In the dry limit of concern here, the liquid volume fraction is essentially 0 and the individual bubbles are polyhedra with curved faces [1] (Fig. 1). Dry foams in equilibrium satisfy Plateau's laws [2]: each film has a constant mean curvature, three films meet along each edge at equal dihedral angles of 120°, and four edges meet at each vertex at the tetrahedral angle of $\cos^{-1}(-\frac{1}{3}) \approx 109.47°$. The Young-Laplace equation, $\Delta p = 4\sigma\mathcal{H}$, relates the mean curvature $\mathcal{H}$ of a film to the pressure difference Δp between neighboring cells; σ is the surface tension and the factor of 4 occurs because each film has two sides.

Diffusive coarsening is a well-known foam aging mechanism that involves pressure-driven gas diffusion through cell walls and an increase in average cell size when shrinking cells disappear. The diffusion is typically slow compared to adjustments in microstructure that maintain mechanical equilibrium (Plateau's laws); consequently, coarsening can be modeled as a quasistatic process in which, typically, large cells grow and small cells shrink and eventually disappear.

In dry two-dimensional (2D) foams, the diffusive growth of each cell is fully described by von Neumann's law,

$$\frac{dA}{dt} = D_2(n-6)\,, \tag{1}$$

where dA/dt is the time derivative of the cells area (A), D_2 is an effective diffusion constant, and n is the number of edges of the cell [3]. This purely topological relation indicates that n captures all of the information on cell shape that affects the growth rate; i.e., all n-edged cells have the same growth rate, even when they are highly deformed. Furthermore, all cells with six edges neither grow nor shrink.

The situation for three-dimensional (3D) foams is more complicated and poorly understood because the dependence of the growth rate of a cell on its shape cannot be expressed as a function of topological features alone [4]. A cell of volume

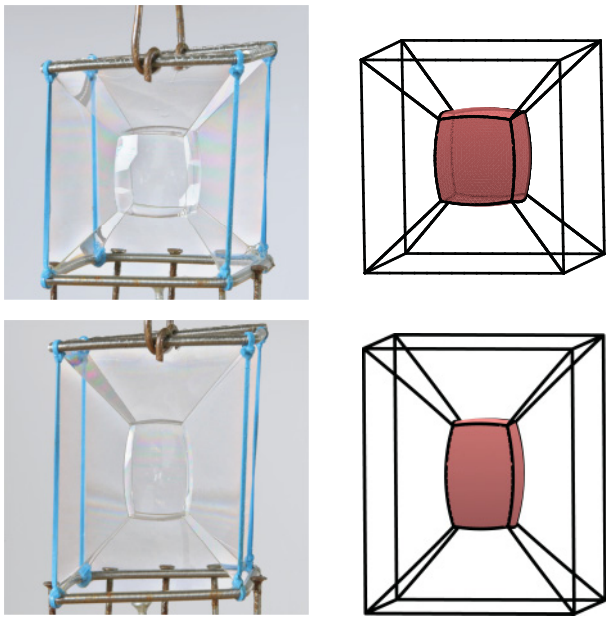

FIG. 1. (Color online) Experimental and simulation snapshots of foam cells with cube topology suspended from wire frames that are "undeformed" (top) and "stretched" (bottom).

*gerd.schroeder-turk@physik.uni-erlangen.de
†klaus.mecke@physik.uni-erlangen.de

V grows or shrinks as

$$V^{-1/3}\frac{dV}{dt} = -DV^{-1/3}\int_{\text{faces}} \mathcal{H}\,dA = -DV^{-1/3}\sum_{i=1}^{F} \mathcal{H}_i S_i = D\mathcal{G}, \tag{2}$$

where D is another effective diffusion coefficient and $\int_{\text{faces}}$ is the integral over the (smooth) faces of the cell, excluding any contribution from the edges. The growth rate $\mathcal{G}$ is a dimensionless function of cell shape only and is proportional to the mean curvature $\mathcal{H}$ integrated over all F faces of the cell [4–6]. The integral can be expressed as a sum that contains the uniform mean curvature $\mathcal{H}_i$ and surface area S_i of each face. This can be understood from the relation between the pressure difference across a film and its mean curvature. The factor $V^{-1/3}$ is introduced in Eq. (2) to give a dimensionless growth rate $\mathcal{G}$ and a coarsening time scale proportional to $V^{2/3}/D$.

Integral geometry can be used to express the integral mean curvature of a domain $\mathbf{D}$ (a foam cell that satisfies Plateau's laws); its relevance to diffusive growth was recognized by Hilgenfeldt *et al.* [6]. The integral mean curvature, in the integral geometry sense, includes the mean curvature located both in the faces and along the sharp edges (cf. Fig. 2); this is a mathematically well-defined quantity despite the curvature discontinuity around the sharp edges. This integral mean curvature over the whole body is known as one of the *intrinsic volumes* of the body, $\pi V_1(\mathbf{D})$, or as the *mean width*, $\pi\mathcal{L}(\mathbf{D})$ [7]. The only quantity relevant to gas diffusion is the integral mean curvature that resides in the faces, which can be expressed as

$$\int_{\text{faces}} \mathcal{H}\,dA = \pi\mathcal{L}(\mathbf{D}) - \frac{\pi}{6}\sum_{i=1}^{n} L_i, \tag{3}$$

where n is the number of edges, and L_i the length of the ith edge. The mean curvature is defined to be the average of the two principal curvatures. The last term represents the integral mean curvature residing in the sharp edges of combined length $\sum_{i=1}^{n} L_i$ (also expressed as $\mathcal{L}(\text{edge}(\mathbf{D}))$ in Ref. [8]) and $\pi/6$ is half the turning angle between adjacent faces. Equation (3) is a direct consequence of simple geometry. The mean width is used in Ref. [8] to give the relation

$$\frac{dV}{dt} = -2\pi M\gamma\left(\mathcal{L}(\mathbf{D}) - \frac{1}{6}\sum_{i=1}^{n} L_i\right), \tag{4}$$

where $M\gamma = D/2$ is the effective diffusion coefficient in this case (the mean curvature here is defined as the sum of the principle curvatures, which accounts for the factor of $1/2$ in the diffusion coefficient). In Ref. [8], this relation is referred to as von Neumann's law generalized to three dimensions; however, it is not topological in nature [9] and simply restates the physical behavior articulated above.

The relation between the topological quantity F and the growth rate has been studied extensively in 3D foams, inspired by the 2D von Neumann's law. An exact 3D analog to von Neumann's law, which relates the growth rate of a cell to topological quantities, alone, does not exist because cells with F faces can have different growth rates $\mathcal{G}$. Consequently, the pursuit of 3D growth laws has focused on statistical relations of the form

$$V_F^{-1/3}\frac{dV_F}{dt} = -DV_F^{-1/3}\left\langle\int \mathcal{H}\,dA\right\rangle = D\mathcal{G}_F, \tag{5}$$

where $\langle\cdot\rangle$ is the average over all F-faced bubbles, and $V_F = \langle V\rangle$. There have been numerous theoretical attempts to find correlations for $\mathcal{G}_F$ [4,6,10,11]. Sire [4] considered *ideal average bubbles* that were semiregular polyhedra with F faces, composed of F_n identical regular spherical faces with n edges ($\sum_{n\geqslant 3} F_n = F$) and derived "almost"-linear expressions for $\mathcal{G}_F$ that compared well with Potts model simulations for which $\mathcal{G}_F$ was considered to be linear [10].

The combination of integral geometry and *idealized bubbles* provided further insight. Hilgenfeldt *et al.* [6] considered an even simpler class of idealized bubbles, regular polyhedra with F identical regular "curved" faces, which can only be realized when $F = 4$, 6, and 12 for the tetrahedron, cube, and dodecahedron, respectively. The integral mean curvature over the body can be expressed as the integral of the *caliper radius* ($\mathcal{C}$), which gives the following expression for the growth rate:

$$\int_{\text{faces}} \mathcal{H}\,dA = \int_{4\pi} \mathcal{C}\,d\omega - \sum_{i=1}^{n}\frac{\pi}{6}L_i, \tag{6}$$

$$\approx \sum_{i=1}^{n}\frac{1}{2}\left(\chi_i - \frac{\pi}{3}\right)L_i, \tag{7}$$

where the caliper radius is integrated over all solid angles $d\omega$, χ_i is the angle between adjacent face normals, and the mean curvature is defined as the average of the principal curvatures. The last, approximate expression was obtained (to leading order in curvature) by evaluating the caliper radius

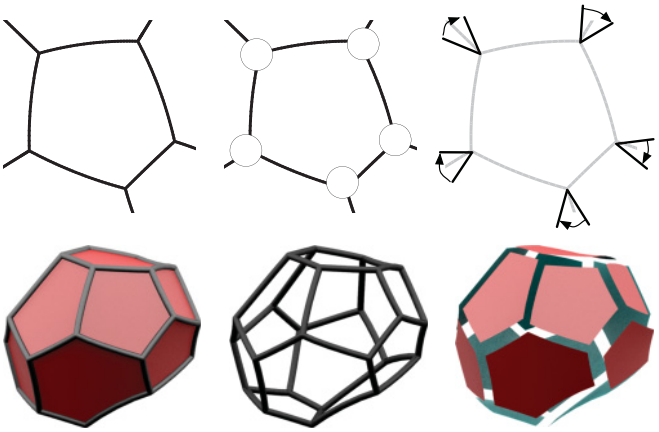

FIG. 2. (Color online) Top: A cell in a 2D foam, which has mean curvature within the edges and mean curvature concentrated at the vertices. Bottom: A cell in a 3D foam, which has mean curvature within the faces as well as mean curvature concentrated along the sharp edges. Only mean curvature within the smooth edges (2D) and faces (3D) contributes to gas diffusion.

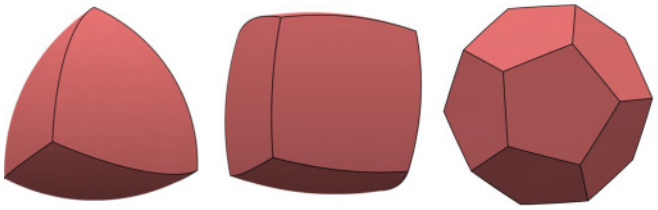

FIG. 3. (Color online) The Constructible IPPs P_4, P_6, and P_{12} are regular polyhedra with spherical-cap faces. Their flat-faced counterparts are the tetrahedron, cube, and dodecahedron. We refer to these cells as regular Platonic foam cells.

for regular polyhedra with flat faces, which resulted in an edge contribution involving χ_i. The growth law that resulted is a nonlinear function of F with *square-root* behavior for large F,

$$\mathcal{G}_F = 2.1431F^{1/2} - 7.7956, \tag{8}$$

which has been shown to be consistent with simulations [6] and experiments [12].

The idealized cells in Ref. [6] were improved on by constructing regular curved polyhedra with F identical *spherical-cap* faces that satisfy Plateau's laws [11]. These *isotropic Plateau polyhedra* (IPPs) provide an analytical expression for $\mathcal{G}_F$, which has $F^{1/2}$ asymptotic behavior

$$\mathcal{G}_F = 2.2129F^{1/2} - 7.7777. \tag{9}$$

The similarity of the two growth laws justifies *a posteriori* the geometric approximations in Ref. [6].

The only realizable IPPs, P_4, P_6, and P_{12}, are curved versions of the regular tetrahedron, cube, and dodecahedron (Fig. 3); they are in fact the only foam cells that can have the topology of Platonic solids because the remaining two Platonic solids, the octahedron and icosahedron, are not trivalent polyhedra and therefore cannot satisfy Plateau's laws. We thus consider *Platonic foam cells* as cells with equivalent topology to P_4, P_6, and P_{12}.

The realizable IPPs, formed as enclosed cells suspended from regular polyhedral wire frames, were indeed known to Plateau and Lamarle [13,14] in the late nineteenth century. Plateau and Lamarle were also aware of the construction of these polyhedra by spherical faces and pointed to further cells that are not Platonic, i.e., composed of different faces; these are a pentagonal and a triangular prism and two other polyhedra composed of both four- and five-sided faces. In a related context, the IPPs have been suggested to describe the shapes of the solid siliceous skeletons of radiolara (single-celled life forms found in oceanic zooplankton) approximately 0.15 mm in size [15,16].

Very little is known about the dependence of growth rate on the shape of 3D foam cells of given topology, which of course is not an issue in two dimensions, where the growth rate depends only on the number of edges. In the remainder of this article we analyze the effect of shape on the growth rate of foam cells of given topology. This is accomplished by considering model systems in which single bubbles are suspended by soap films from rigid wire frames whose (undeformed) shape is inherited from the corresponding Platonic solid; i.e., cube bubbles are suspended from wire frames with the topology of a cube, as shown in Fig. 1. We refer to the bubbles as foam cells because they satisfy Plateau's laws when the total surface area of the soap films—those that bound the bubble as well as the supporting films—is minimized. We note, however, that the bubbles are surrounded by uniform pressure, which means that the pressure differences across each cell face are equal, and therefore, the mean curvatures are also equal. This construction allows us to distinguish the effect of shape from the qualitatively different situation in real, disordered foams, where the pressures in all the neighboring cells are, in general, different because of their configuration in the foam. Bubble distortions are induced through extension, compression, shear, and torsion of the wire frames. The Surface Evolver is used to model the film geometry.

II. 2D FOAM CELL IN A RECTANGULAR FRAME

It is instructive to consider a representative cell deformation in two dimensions even though—by von Neumann's law—the growth rate is unaffected when the number of edges is unchanged. The quadrilateral foam cell under consideration (shown in Fig. 4) is the 2D counterpart of the cubic Platonic cell (shown in Figs. 1 and 3). The planar cell is at equilibrium (satisfies Plateau's laws), has unit area $A = 1$ and four curved films (edges); the cell vertices are connected to fixed points $(\pm L/2, \pm\delta L/2)$ (Fig. 4) on the corners of a rectangle, by films that are also subject to length minimization. The pressure outside the cell is *constant* so all four edges are circular segments with the same radius of curvature R centered at $(\pm x_0, 0)$ and $(0, \pm y_0)$. A convenient parametrization for different values of δ

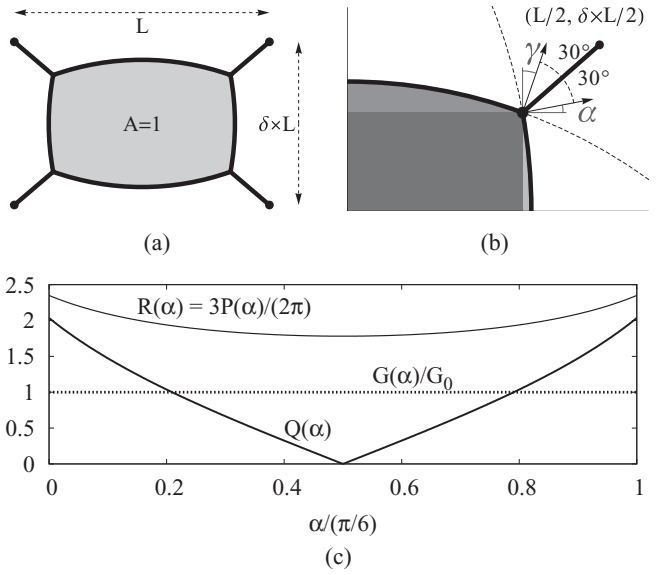

FIG. 4. Planar four-sided foam cell in a rectangular frame. (a) Quadrilateral cell suspended in a rectangle of size $L \times (\delta L)$. (b) Parametrization of cell deformations in terms of α yields analytical expressions for all relevant quantities. (c) The cell deformation Q, growth rate $\mathcal{G}$ relative to the growth rate $\mathcal{G}_0$ of the isotropic cell ($\alpha = \pi/12$), and radius of curvature R of the cell edges, as functions of α.

is provided by the angle $\alpha \in [0,\pi/6]$, which is measured from the horizontal axis to the normal of the "vertical" film at the top right vertex (see Fig. 4). Using Plateau's law (written as $\pi/3 + \alpha + \gamma = \pi/2$; see Fig. 4) and requiring the cell area to be 1, one obtains

$$R = \frac{\sqrt{6}}{\sqrt{3\sin(2\alpha) + 3\sqrt{3}\cos(2\alpha) + 2\pi - 6\sqrt{3}}} \tag{10}$$

for the radius and

$$x_0 = -\frac{\sqrt{3}\sin(\alpha) + \cos(\alpha)}{\sqrt{2\sin(2\alpha) + 2\sqrt{3}\cos(2\alpha) + \frac{4\pi}{3} - 4\sqrt{3}}}, \tag{11}$$

$$y_0 = \frac{\sqrt{3}\sin(\alpha) - 3\cos(\alpha)}{\sqrt{6(\sin(2\alpha) + \sqrt{3}\cos(2\alpha) - 2\sqrt{3}) + 4\pi}} \tag{12}$$

for the center-point coordinates, $(\pm x_0,0)$ and $(0, \pm y_0)$, of the circles that define the films.

In line with von Neumann's law, one finds that the total length P of the four cell edges (the perimeter) is proportional to the radius of curvature, $P = (2\pi/3)R$. Therefore, the cell growth rate $\mathcal{G} \propto \int_B \kappa dr = P/R = 2\pi/3$ is constant for any deformation measured by α or δ; B is the cell boundary and κ is the local film curvature. The invariance of growth rate to cell deformation is in stark contrast to the 3D situation discussed below.

Note that changing α results in a genuine cell deformation, which is conveniently quantified by the traceless interface tensor $q_{ij} = A^{-1/2}\int_B [\frac{1}{2}\delta_{ij} - n_i n_j]dr$, where δ_{ij} is the Kronecker δ and n_i $(i = 1,2)$ are the components of the local film normal vector. The scalar measure of cell distortion defined by

$$Q = \left(\sum_i \sum_j \frac{1}{2} q_{ij}\, q_{ij}\right)^{\frac{1}{2}}$$

is given by

$$Q = \sqrt{6}\sqrt{\frac{\left(\cos\left(2\alpha + \frac{\pi}{6}\right) - \sin(2\alpha)\right)^2}{3\sin(2\alpha) + 3\sqrt{3}\cos(2\alpha) + 2\pi - 6\sqrt{3}}}. \tag{13}$$

Figure 2 demonstrates that Q takes on finite positive values when α differs from $\pi/12$. The plot also shows the radius of curvature R and emphasizes that the growth rate $\mathcal{G}$ is independent of the degree of cell distortion. The symmetry of the curves with respect to $\alpha = \pi/12$ is a reflection of the fact that the cells for α and $\pi/6 - \alpha$ are rotations of each other by $\pi/2$.

The variable α can be used to parametrize the problem because only the angle formed by the four films that suspend the foam cell from the rectangular corners affects its shape; the length of the suspending films is irrelevant because they are straight. By contrast, for most of the deformations of 3D cells discussed below, both the size and the aspect ratio of the wire frame affect the bubble shape and growth rate.

III. MODELING DEFORMED PLATONIC FOAM CELLS WITH THE SURFACE EVOLVER

The Surface Evolver is a software tool developed by Kenneth Brakke for the minimization of surface energy functionals subject to constraints [17]. We generate models of the Platonic foam cells suspended by films from fixed wire frames whose (undeformed) shapes are inherited from regular polyhedra, i.e., the tetrahedron, cube, and dodecahedron (Fig. 5). Each (undeformed) wire-frame segment has equal length $L > 1$, the normalized edge length of the initial undeformed cell. The central body before area minimization is a regular polyhedron with flat faces and unit edge length, which determines the volume constraint. For these underformed isotropic cases, when the surface area is minimized, the body approximates a regular (isotropic) Platonic foam cell (Fig. 3), equivalent to the realizable IPPs of Ref. [11]. For these isotropic cases, the cell shape is independent of the wire-frame size L because the supporting films are flat, by symmetry.

Cell distortion is induced by "deforming" the wire frame to mimic extension, compression, shear, and torsion, while maintaining straight wire-frame components. All of the wire-frame deformation modes and relative orientations are illustrated in Fig. 6 and specified in the Appendix. Imagine that a wire frame is attached to a pair of rigid horizontal planes. The tetrahedral frame is oriented so that only one strut lies in each plane and the other frames are oriented to minimize the distance between the planes. Extension and compression are accomplished by increasing and decreasing, respectively, the plane separation. Shear is induced by sliding the planes in opposite directions, parallel or perpendicular to the fixed edges of the tetrahedron and cube or perpendicular to one of the fixed edges of the dodecahedron on each plane. Torsion corresponds to rotation of both planes in opposite directions around the central axis of each wire frame. In the case of the dodecahedron, half of the wire-frame vertices lie in between the planes. During torsion, these vertices are moved by a linear interpolation of the rotation from the midplane; however, for extension, compression, and shear these vertex positions are fixed. This set of deformations is not complete by any means but does enable us to explore the effect of cell shape on growth rate for representative deformation modes.

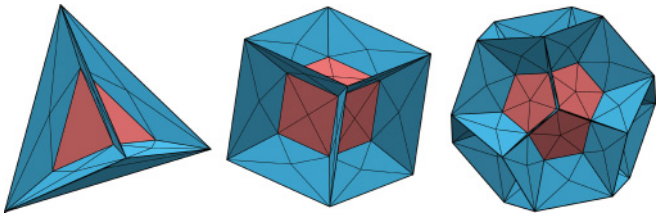

FIG. 5. (Color online) Illustration of the Platonic foam cell models. The interior (red) soap films bound a body of fixed volume suspended by (blue) films from a fixed wire frame. All of the soap films (facets) are free to move during surface area minimization.

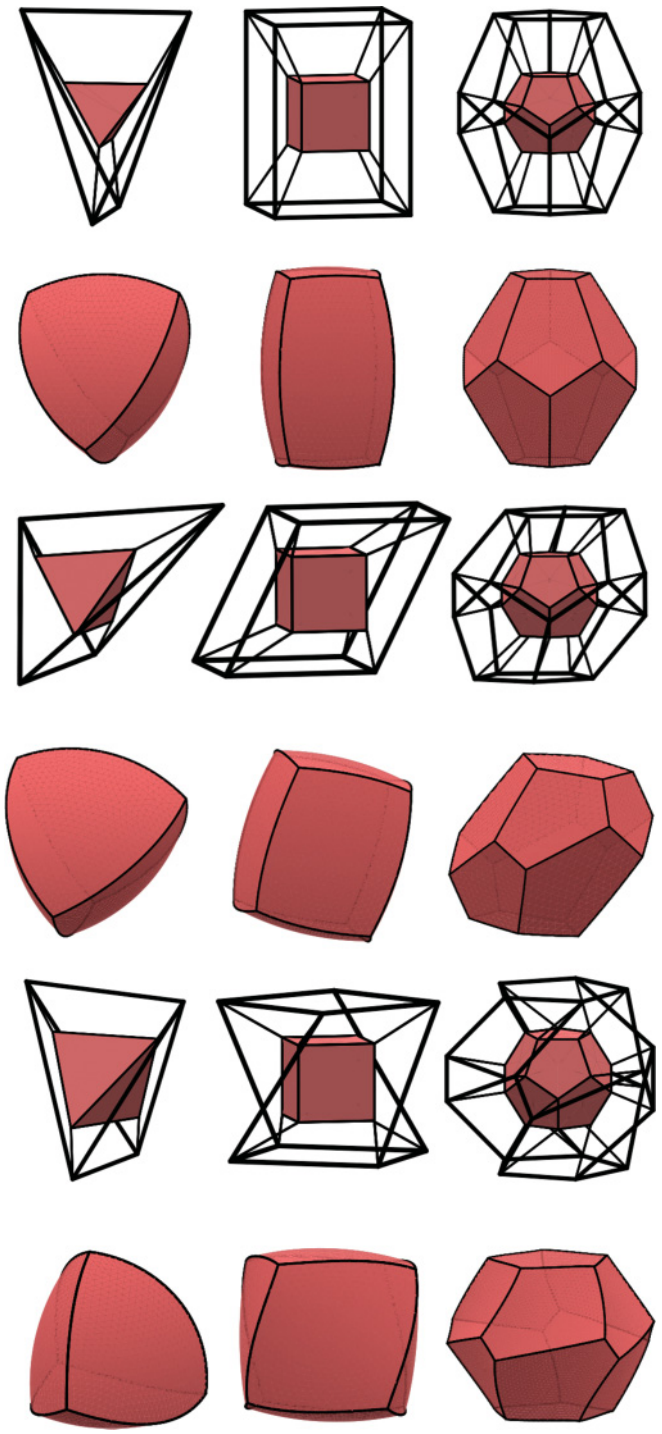

FIG. 6. (Color online) Deformation of the wire frames and the corresponding deformed foam cells: (top) extension, (middle) shear, and (bottom) torsion for tetrahedral (left), cubic (center), and dodecahedral (right) foam cells.

When the wire frame is deformed and the total film area is minimized, the foam cell responds by satisfying Plateau's laws. The surfaces whose area is collectively minimized include the films bounding the Platonic foam cell as well as the films that attach the cell to the wire frame. The supporting films must have zero mean curvature because they all reside in the uniform pressure environment outside the cell; however, they are not necessarily flat when the wire frame is deformed and can, in fact, be highly curved. The mean curvature is uniform over the enclosed cell surface; the mean curvature and surface area of each face are provided by the Surface Evolver.

The geometry of the supporting films and the bubble shape both depend on the size L of the deformed wire frames, in sharp contrast to the 2D situation discussed in Sec. II. We use, as a direct measure of cell distortion, the dimensionless scalar Q, which is defined as [18]

$$Q = \left(\sum_i \sum_j \frac{1}{2} q_{ij} q_{ij} \right)^{1/2}, \tag{14}$$

where

$$q_{ij} = V^{-2/3} \int_{\text{faces}} \left(\frac{1}{3}\, \delta_{ij} - n_i n_j \right) dA, \tag{15}$$

and the n_i are components of the pointwise normal vector on the surface. In a different context, q_{ij} is a close relative of the Minkowski tensors $W_\nu^{r,s}$ used as robust shape measures for microstructured materials [19,20].

IV. GROWTH RATE TRENDS WITH DEFORMATION

We examine the relationship between the diffusive growth rate and the shape of deformed foam cells for a range of wire-frame sizes for each deformation mode. The regular (undeformed) Platonic foam cells all shrink and therefore have negative growth rates of $\mathcal{G}_0 \approx -3.966$, -2.850, and -0.4530 for the tetrahedron, cube, and dodecahedron, respectively [11]. The growth rates of deformed cells are shown in Fig. 7.

Extension and compression cause the relative growth rate $\mathcal{G}/\mathcal{G}_0$ of cubic and dodecahedral cells to increase; i.e., the cells shrink faster. However, tetrahedral cells exhibit the opposite response: the relative growth rate decreases. The distortion of tetrahedral cells in compressed wire frames is negligible, and thus the results are omitted from Fig. 7. Torsion causes the relative growth rate to decrease (except for extremely small increases for cubic cells in large frames).

Two factors contribute to the growth rate of these foam cells: their surface area (S) and the mean curvature of their faces ($\mathcal{H}$). Table I reports how these quantities vary with deformation relative to the isotropic cell. Torsion and shear cause $\mathcal{H}/\mathcal{H}_0$ to decrease; however, there is no consistency across the other combinations of deformation and cell type. The surface area of a cell increases with deformation in all cases except one: torsion of the cubic cell. A cubic cell deformed by torsion is shown in Fig. 8, along with a plot of S vs Q, which shows that S decreases for small wire frames ($L < 3$). This indicates that the isotropic cubic foam cell (the IPP) does not have the lowest surface area.

The response of dodecahedral cells to torsion in small wire frames is particularly noteworthy because the growth rate, and therefore the mean curvature, eventually changes sign; i.e., the foam cells grow. The cause of the sign change in the mean curvature is unclear. This and the relevance of

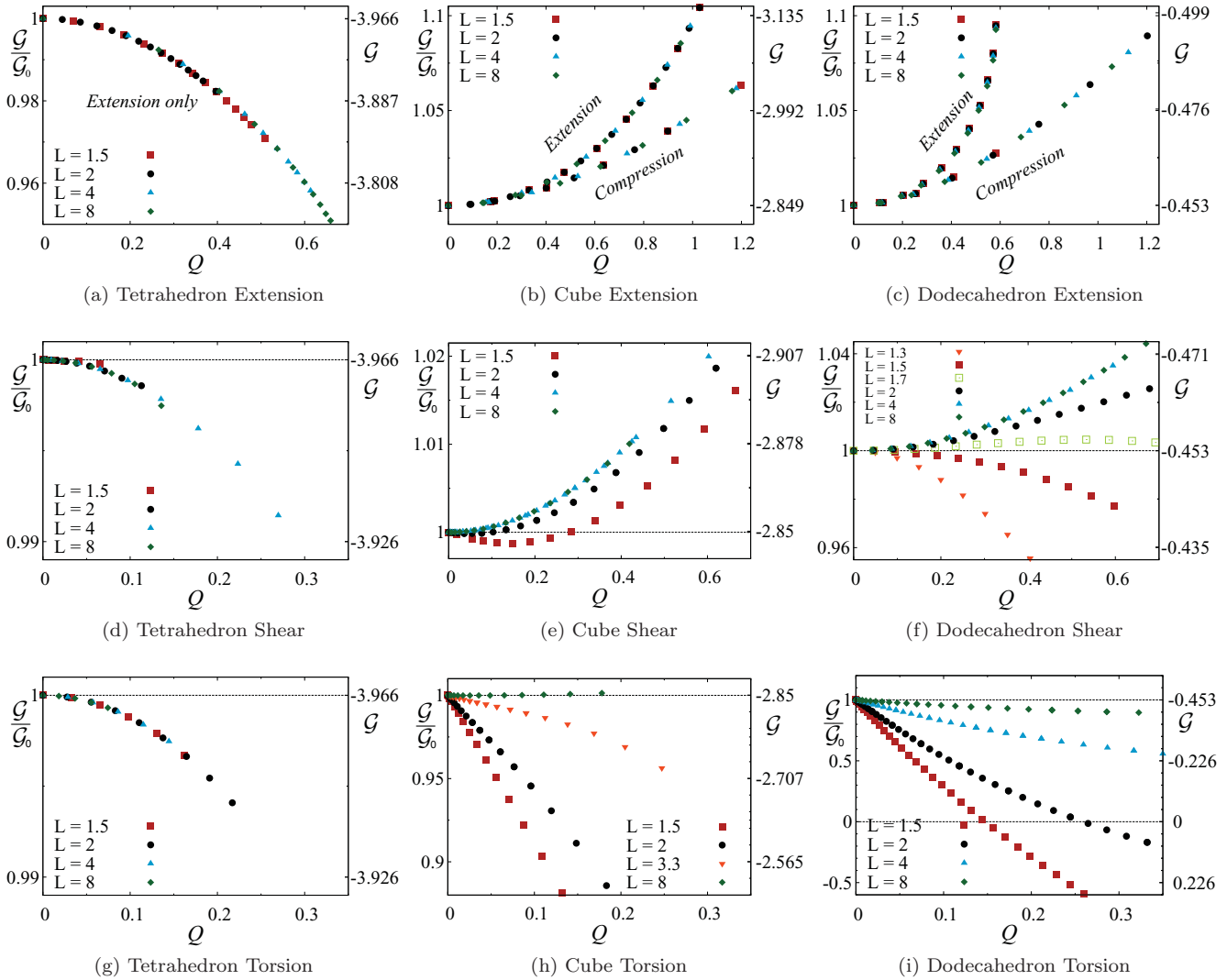

FIG. 7. (Color online) Growth rate $\mathcal{G}$ as a function of Q for the three Platonic foam cells. The left y axis shows the relative growth rate $\mathcal{G}/\mathcal{G}_0$; the right y axis, the absolute growth rate $\mathcal{G}$. The value of $\mathcal{G}_0$ is approximately -3.966, -2.850, and -0.4530 for the tetrahedron, cube, and dodecahedron, respectively. The parameter L is the wire-frame size. Under compression the tetrahedral cell experiences negligible distortion, so the results are omitted.

torsional deformations in real (disordered) foams offer food for thought.

The dependence of growth rate on frame size is particularly evident for the dodecahedral cell under shear because the growth rate can significantly increase or decrease with Q. The variation in growth rate trends for different frame sizes indicates that the resulting cell shapes are qualitatively different and cannot be distinguished by the measure Q.

Extension and compression are interesting deformation modes because the dependence of the growth rate on Q is virtually independent of the wire-frame size. This suggests that the shape of the foam cell and the suspending films in its vicinity are relatively insensitive to the frame size. All deformations of the tetrahedral cell are also independent of the wire-frame size, within numerical accuracy.

V. EXPERIMENTAL DEFORMATION OF CUBIC FOAM CELLS

Physical realizations of deformed cubic cells are built by suspending soap films from a deformable wire frame, reminiscent of experimental cells in Ref. [21]. Extension, compression, shear, and torsion were accomplished experimentally and recreated as Surface Evolver models.

The cubic wire frame was constructed from threaded metal rods (6.2 cm long and 2 mm in diameter) joined together to form two rigid squares, which were then connected by elastic bands to enable a variety of deformations. The longevity of the bubble was increased when threaded rods were used, as the threads held additional soap solution. A wire handle was attached to one of the rigid squares.

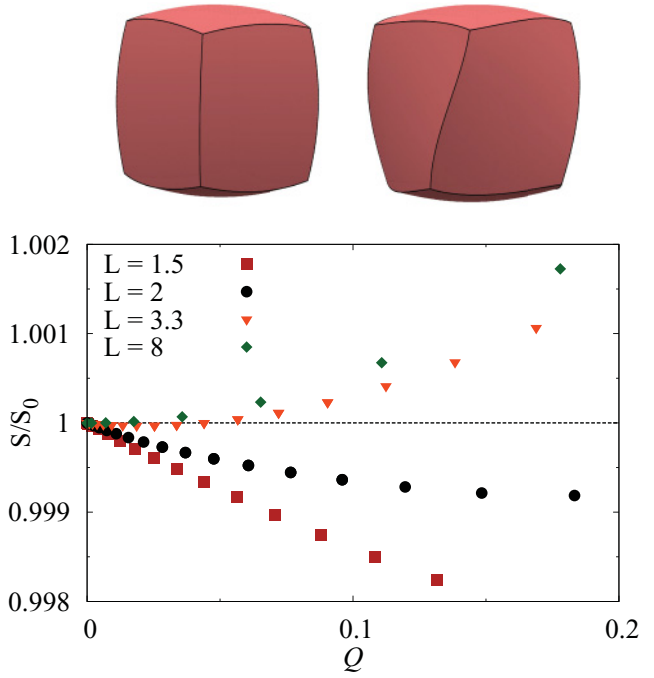

FIG. 8. (Color online) Surface area S vs deformation Q for a cubic foam cell under torsion (shown above). S_0 refers to the regular cube foam cell; i.e., the cube IPP.

The soap solution contains 900 ml distilled water, 250 ml perfume-free liquid detergent, and 3–5 g dry wallpaper glue powder (wheat paste). After mixing, the solution was rested for 2 days before use. The suspended bubble is created by dipping the frame into the solution twice. After the first dip, a square film forms in the middle of the frame, and after the second, a gas bubble is trapped between the square film and the solution surface. Figure 9 shows three deformations of a suspended cubic bubble under torsion, compression, and shear. This experiment provides evidence that the deformation of suspended soap bubbles is physically realizable.

TABLE I. Changes in surface area S, relative mean curvature $\mathcal{H}/\mathcal{H}_0$, and relative growth rate $\mathcal{G}/\mathcal{G}_0$ with increasing deformation Q.

	S	$\mathcal{H}/\mathcal{H}_0$	$\mathcal{G}/\mathcal{G}_0$	Notes
Tetrahedron				
Extension	↑	↓	↓	
Shear	↑	↓	↓	
Torsion	↑	↓	↓	
Cube				
Extension	↑	↑	↑	
Compression	↑	↓	↑	
Shear	↑	↓	↑	For $L < 2$, $\mathcal{G}/\mathcal{G}_0$ is not monotonic.
Torsion	↓	↓	↓	For $L > 3$, S increases.
Dodecahedron				
Extension	↑	↑	↑	
Compression	↑	↓	↑	
Shear	↑	↓	↑	For $L < 1.7$, $\mathcal{G}/\mathcal{G}_0$ decreases.
Torsion	↑	↓	↓	

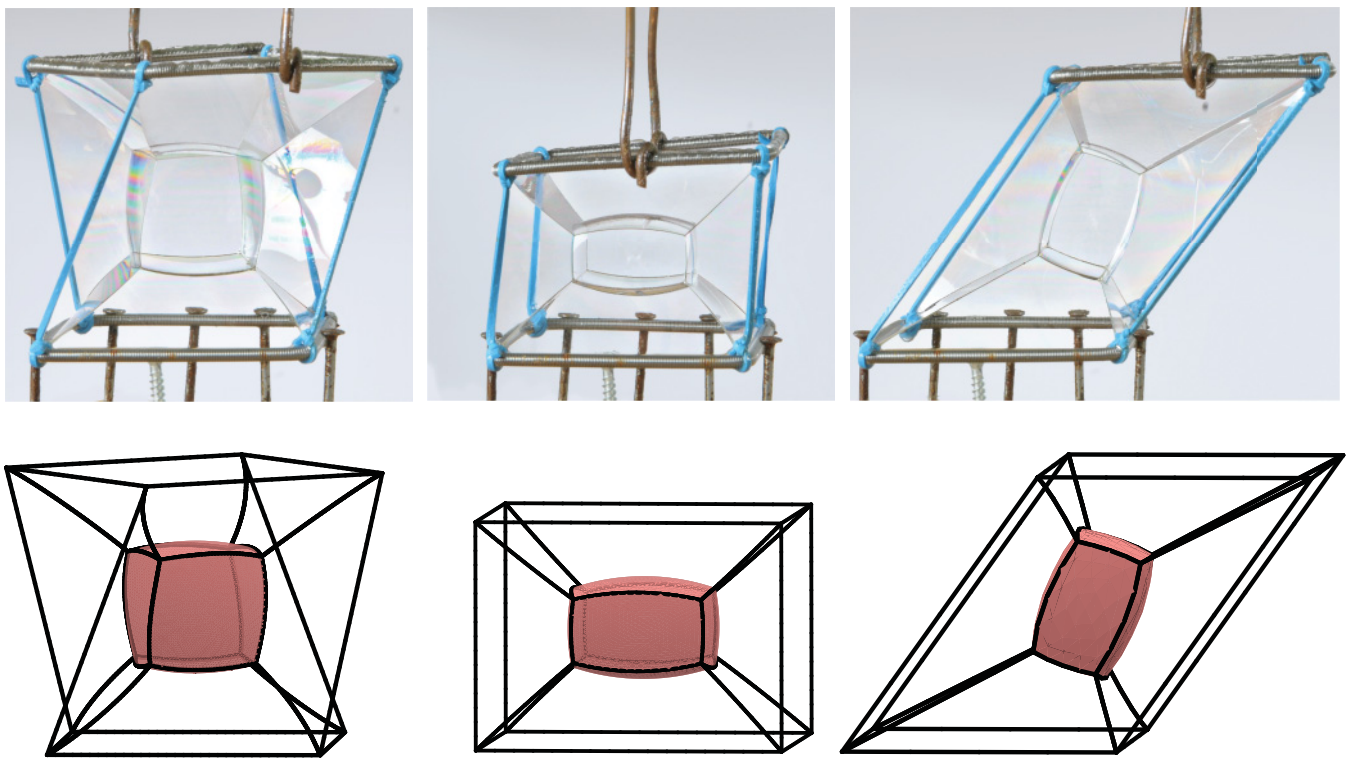

FIG. 9. (Color online) Experimental and simulated images of soap bubbles suspended from initially cubic wire frames that are subjected to torsion (left), compression (center), and shear (right). Simulations indicate that the surface area of a cubic bubble decreases under torsion; see Fig. 8.

VI. DISCUSSION AND CONCLUSIONS

We have shown that the diffusive growth rate of 3D foam cells of given topology varies with cell shape by examining deformations of three cells with a very simple topology; these Platonic foam cells, even when deformed, satisfy Plateau's laws and are based on the trivalent Platonic solids (tetrahedron, cube, and dodecahedron). This change in the growth rate with geometric distortion for 3D foam cells is in contrast to 2D foams, where the growth rate of cells with the same number of edges does not depend on the shape, according to von Neumann's law.

The Surface Evolver is used to model the distortion of single foam cells that are suspended from wire frames by soap films. Cell distortion is induced by deforming the wire frame to mimic extension, compression, shear, and torsion. The growth rate of deformed Platonic foam cells can be greater than or less than the growth rate of the regular undeformed cells.

The growth rate of the regular Platonic foam cells is negative and therefore they shrink. The response of dodecahedral cells under torsion of small wire frames is particularly noteworthy because the growth rate, and therefore the mean curvature, eventually changes sign; i.e., the foam cells grow. The cause of the sign change in the mean curvature is unclear.

The response of the model wire-frame system is relatively complicated because the geometry of the bubble and the suspending films are coupled through the minimization of their combined surface area. Consequently, the dependence of the shape of the foam cell on the size and shape (deformation mode) of the wire frame is difficult to gauge, in general. However, many of the deformations are noteworthy because the dependence of growth rate on cell distortion is virtually independent of the wire-frame size, which suggests that the shape of the foam cell and the suspending films in its vicinity do not depend on the wire-frame size. The cause of this similarity in shape is not obvious and is worthy of investigation.

Figure 10 shows all of the growth rates in Fig. 7 plotted against the mean curvature in the sharp edges of the cells.

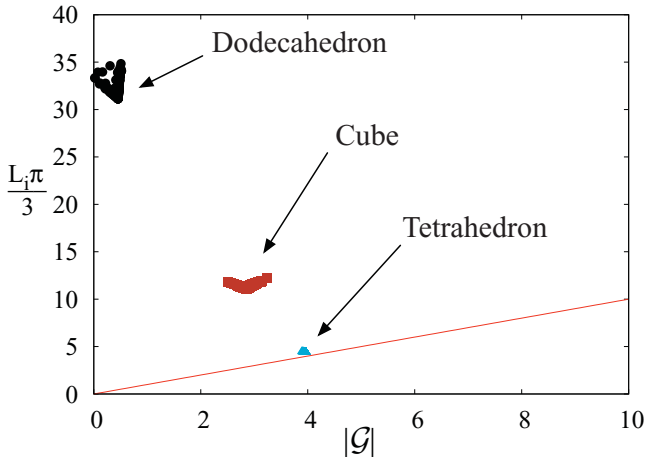

FIG. 10. (Color online) All of the growth rates in Fig. 7 plotted against the mean curvature in the sharp edges of the cells.

TABLE II. Some Q values for given δ values. All are with frame size $L = 2$

	Tetrahedron	Cube	Dodecahedron
Extension, $\delta = 0.4$	0.0857	0.3306	0.2011
Shear, $\delta = 1$	0.0775	0.2041	0.2300
Torsion, $\delta = 0.7$	0.1911	0.0110	0.0140

First, the variation in $\mathcal{G}$ caused by changing the shape of each type of cell is significant. Second, the magnitude of $\mathcal{G}$ (corresponding to the mean curvature integrated over the faces only) is much smaller than the mean curvature in the sharp edges—particularly so for the dodecahedral cells, where $\mathcal{G}$ can vanish. Thus, the contribution of the edges $\sum L_i \frac{\pi}{3}$ to $\mathcal{L}(\mathbf{D})$ far outweighs the physically relevant contribution of the faces. The quantity $\mathcal{L}(\mathbf{D})$ is amenable to improved analysis by integral geometry, but for foam cells it is not useful when computing cell growth rates, in contrast to the suggestion in Ref. [8].

The purpose of this paper is to show that deforming cells with a given topology changes the growth rate, so shape really does matter. In real foams, the surrounding bubbles have different pressures, making them a far more complex ensemble. It is thus very difficult to speculate on the effect of shape within real foams and, also, to relate L to the size of the neighboring bubbles in any obvious way. A further complication to this would be polydispersity in a random foam. Regardless, we see our analysis as a step towards a deeper understanding of the complex and varied relationship between cell shape and growth rate in foams.

ACKNOWLEDGMENTS

We acknowledge support from the German research foundation (DFG) through the research group Geometry and Physics of Spatial Random Systems under Grants No. SCHR1148/3-1 and ME1361/12-1. We acknowledge the DFG cluster of excellence Engineering of Advanced Materials (EAM) at the University of Erlangen for supporting several visits to Erlangen by Andrew Kraynik. We thank Sebastian Kapfer, Sascha Hilgenfeldt, and Christophe Oguey for comments, Kenneth Brakke for his freely available Surface Evolver software, and Tabea Hartmann for the photographs in Figs. 1 and 9.

APPENDIX: SURFACE EVOLVER SIMULATIONS

The cell deformations examined in this paper were simulated using the Surface Evolver. The cells were suspended from fixed wire frames, as shown in Fig. 6. Table II lists some typical values of the cell deformation measure Q for differing values of the wire-frame deformation parameter δ. Table III lists the initial vertex positions of the suspended cell and defines the vertex positions of the fixed wire frame given the size of the wire frame L and the deformation parameter δ.

TABLE III. Fixed wire-frame vertex positions. $\{W_x, W_y, W_z\}$ are the positions of the fixed vertices of the wire frame given the cell vertices $\{x, y, z\}$ and are specified for a deformation given a frame size L and a deformation parameter δ.

	Tetrahedron ($b = 0.5\sqrt{0.5}$)
Cell	$\{b,b,b\}$, $\{-b,-b,b\}$, $\{-b,b,-b\}$, $\{b,-b,-b\}$
Extension	$\{W_x,W_y,W_z\} = \{xL, yL, z(L + \frac{\delta}{2\lvert z\rvert})\}$
Shear	$\{W_x,W_y,W_z\} = \{xL + \frac{z}{\lvert z\rvert}\frac{\delta}{2\sqrt{2}}, yL + \frac{z}{\lvert z\rvert}\frac{\delta}{2\sqrt{2}}, zL\}$
Torsion	$\{W_x,W_y,W_z\} = \{xL\cos(\frac{z}{\lvert z\rvert}\frac{\delta}{2}) - yL\sin(\frac{z}{\lvert z\rvert}\frac{\delta}{2}), xL\sin(\frac{z}{\lvert z\rvert}\frac{\delta}{2}) + yL\cos(\frac{z}{\lvert z\rvert}\frac{\delta}{2}), zL\}$
	Cube ($b = 0.5$)
Cell	$\{-b,-b,-b\}$, $\{b,-b,-b\}$, $\{b,b,-b\}$, $\{-b,b,-b\}$, $\{-b,-b,b\}$, $\{b,-b,b\}$, $\{b,b,b\}$, $\{-b,b,b\}$
Extension	$\{W_x,W_y,W_z\} = \{xL, yL, z(L + \frac{\delta}{2\lvert z\rvert})\}$
Shear	$\{W_x,W_y,W_z\} = \{xL, yL + \frac{z}{\lvert z\rvert}\frac{\delta}{2}, zL\}$
Torsion	$\{W_x,W_y,W_z\} = \{xL\cos(\frac{z}{\lvert z\rvert}\frac{\delta}{2}) - yL\sin(\frac{z}{\lvert z\rvert}\frac{\delta}{2}), xL\sin(\frac{z}{\lvert z\rvert}\frac{\delta}{2}) + yL\cos(\frac{z}{\lvert z\rvert}\frac{\delta}{2}), zL\}$
	Dodecahedron ($s = (1 + \sqrt{5})/4$)
Cell	$\{0, -\frac{1}{2}, -2s^2\}$, $\{s,-s,-s\}$, $\{2s^2, 0, -\frac{1}{2}\}$, $\{s,s,-s\}$, $\{0, \frac{1}{2}, -2s^2\}$ vertices on the upper face, attached to the upper rigid horizontal plane, distance $d \approx 1.1135$ from the midplane. Normal vector $[0.5257, 0, -0.8507] = [\eta_1,\eta_2,\eta_3]$ $\{-s,-s,s\}$, $\{0, -\frac{1}{2}, 2s^2\}$, $\{0, \frac{1}{2}, 2s^2\}$, $\{-s,s,s\}$, $\{-2s^2, 0, \frac{1}{2}\}$ vertices on the lower face, attached to the bottom rigid horizontal plane, distance $d \approx 1.1135$ from the midplane $\{-s,-s,-s\}$, $\{\frac{1}{2}, -2s^2, 0\}$, $\{2s^2, 0, \frac{1}{2}\}$, $\{\frac{1}{2}, 2s^2, 0\}$, $\{-s,s,-s\}$ central vertices closer to the upper plane, distance $d \approx 0.2629$ from the midplane $\{-\frac{1}{2}, -2s^2, 0\}$, $\{s,-s,s\}$, $\{s,s,s\}$, $\{-\frac{1}{2}, 2s^2, 0\}$, $\{-2s^2, 0, -\frac{1}{2}\}$ central vertices closer to the lower plane, distance $d \approx 0.2629$ from the midplane
Extension	Vertices ($d = 1.1135L$): $\{W_x,W_y,W_z\} = \{xL + \eta_1\delta, yL, zL + \eta_3\delta\}$ Vertices ($d = -1.1135L$): $\{W_x,W_y,W_z\} = \{xL - \eta_1\delta, yL, zL - \eta_3\delta\}$ Vertices ($d = \pm 0.2629L$): $\{W_x,W_y,W_z\} = \{xL, yL, zL\}$
Shear	Shear direction $[0.6882, 0.5888, 0.4253] = [s_1,s_2,s_3]$ Vertices ($d = 1.1135L$): $\{W_x,W_y,W_z\} = \{xL + s_1\delta, yL + s_2\delta, zL + s_3\delta\}$ Vertices ($d = -1.1135L$): $\{W_x,W_y,W_z\} = \{xL - s_1\delta, yL - s_2\delta, zL - s_3\delta\}$ Vertices ($d = \pm 0.2629L$): $\{W_x,W_y,W_z\} = \{xL, yL, zL\}$
Torsion	$R(\delta)$ = Rotation matrix around $[\eta_1,\eta_2,\eta_3]$ through center of upper face $[0.58541, 0, -0.94721]$ by an angle δ Vertices ($d = 1.1135L$): apply $R(\frac{\delta}{2})$ to give fixed wire-frame vertices Vertices ($d = -1.1135L$): apply $R(-\frac{\delta}{2})$ to give fixed wire-frame vertices Vertices ($d = \pm 0.2629L$): apply $R(\pm 0.2361 \times \frac{\delta}{2})$ to give fixed wire-frame vertices

[1] D. Weaire and S. Hutzler, *The Physics of Foams* (Clarendon Press, Oxford, UK, 1999).

[2] J. Plateau, *Statique Experimentale et Theorique des Liquides* (Gauthier-Villiard, Paris, 1873).

[3] J. von Neumann, *Metal Interfaces* (American Society for Metals, Cleveland, 1952), pp. 108–110.

[4] C. Sire, Phys. Rev. Lett. **72**, 420 (1994).

[5] W. W. Mullins, J. Appl. Phys. **59**, 1341 (1986).

[6] S. Hilgenfeldt, A. M. Kraynik, S. A. Köhler, and H. A. Stone, Phys. Rev. Lett. **86**, 2685 (2001).

[7] R. Schneider and W. Weil, *Stochastic and Integral Geometry* (Springer-Verlag, Berlin, 1993).

[8] R. D. MacPherson and D. J. Srolovitz, Nature **446**, 1053 (2007).

[9] M. Elsey, S. Esedoḡlu, and P. Smereka, Proc. R. Soc. A **467**, 381 (2010).

[10] J. A. Glazier, Phys. Rev. Lett. **70**, 2170 (1993).

[11] S. Hilgenfeldt, A. M. Kraynik, D. J. Reinelt, and J. Sullivan, Europhys. Lett. **67**, 484 (2004).

[12] J. Lambert, R. Mokso, I. Cantat, P. Cloetens, J. A. Glazier, F. Graner, and R. Delannay, Phys. Rev. Lett. **104**, 248304 (2010).

[13] J. A. F. Plateau, Ann. Phys. **204**, 477 (1866).

[14] E. Lamarle, Mémoires de l'Académie Royale de Belgique **35**, 3 (1864).

[15] D. Thompson, *On Growth and Form* (Cambridge University Press, Cambridge, 1917).

[16] E. Haeckel and O. Breidbach, *Art Forms from the Ocean: The Radiolarian Atlas of 1862* (Prestel, London, 2005).

[17] K. Brakke, Exp. Math. **1**, 141 (1992).

[18] A. M. Kraynik, D. A. Reinelt, and F. van Swol, Phys. Rev. E **67**, 031403 (2003).

[19] C. H. Arns, M. Knackstedt, and K. Mecke, J. Microsc. **240**, 181 (2010).

[20] G. E. Schröder-Turk, W. Mickel, S. C. Kapfer, M. A. Klatt, F. M. Schaller, M. J. Hoffmann, N. Kleppmann, P. Armstrong, A. Inayat, D. Hug, M. Reicheldorfer, W. Peukert, W. Schwieger, and K. Mecke, Adv. Mater. **23**, 2535 (2011).

[21] P. Ball, *The Self-Made Tapestry: Pattern Formation in Nature* (Oxford University Press, New York, 1999).